Acta Biomaterialia xxx (xxxx) xxx

Contents lists available at ScienceDirect

Acta Biomaterialia

journal homepage: www.elsevier.com/locate/actbio

Full length article

# Polyphenol-modified biomimetic bioadhesives for the therapy of annulus fibrosus defect and nucleus pulposus degeneration after discectomy

Yan Ju[a], Shiyuan Ma[a], Meimei Fu[a], Min Wu[a], Yue Li[a,b], Yue Wang[a], Meihan Tao[a,*], Zhihui Lu[a,c,*], Jinshan Guo[a,c,d,*]

[a] Department of Histology and Embryology, NMPA Key Laboratory for Safety Evaluation of Cosmetics, School of Basic Medical Sciences, Guangdong Provincial Key Laboratory of Bone and Joint Degeneration Diseases, The Third Affiliated Hospital of Southern Medical University, Southern Medical University, Guangzhou 510515, PR China
[b] Department of Plastic and Aesthetic Surgery, Nanfang Hospital of Southern Medical University, Guangzhou 510515, PR China
[c] Regenerative Medicine and Tissue Repair Material Research Center, Huangpu Institute of Materials, 88 Yonglong Avenue of Xinlong Town, Guangzhou 511363, PR China
[d] CAS Key Laboratory of High-Performance Synthetic Rubber and its Composite Materials, Changchun Institute of Applied Chemistry, Chinese Academy of Sciences, 5625 Renmin Street, Changchun 130022, PR China

ARTICLE INFO

*Article history:*
Received 11 June 2024
Revised 29 August 2024
Accepted 22 September 2024
Available online xxx

*Keywords:*
Bioadhesives
Polyphenol
Annulus fibrosus
Nucleus pulposus
Discectomy

ABSTRACT

Discectomy is the surgical standard of care to relieve low back pain caused by intervertebral disc (IVD) herniation. However, there remains annulus fibrosus (AF) defect and nucleus pulposus (NP) degeneration, which often result in recurrent herniation (re-herniation). Herein, we develop a polyphenol-modified waterborne polyurethane bioadhesives (PPU-glues) to promote therapy prognosis after discectomy. Being composed of tannic acid (TA) mixed cationic waterborne polyurethane nanodispersions (TA/WPU$^+$) and curcumin (Cur) embedded anionic waterborne polyurethane nanodispersions (Cur-WPU$^-$), PPU-glue gels rapidly (<10 s) and exhibits low swelling ratios, tunable degradation rates and good biocompatibility. Due to the application of an adhesion strategy combing English ivy mechanism and particle packing theory, PPU-glue also shows considerable lap shear strength against wet porcine skin (≈58 kPa) and burst pressure (≈26 kPa). The mismatched particle sizes and the opposite charges of TA/WPU$^+$ and Cur-WPU$^-$ in PPU-glue bring electrostatic interaction and enhance particle packing density. PPU-glue possesses superior reactive oxygen species (ROS)-scavenging capacity derived from polyphenols. PPU-glue can regulate extracellular matrix (ECM) metabolism in degenerated NP cells, and it can promote therapy biologically and mechanically in degenerated rat caudal discs. In summary, this study highlights the therapeutic approach that combines AF seal and NP augmentation, and PPU-glue holds great application potentials for post discectomy therapy.

**Statement of significance**

Currently, there is no established method for the therapy of annulus fibrosus (AF) defect and nucleus pulposus (NP) degeneration after discectomy. Herein, we developed a polyphenol-modified biomimetic polyurethane bioadhesive (PPU-glue) with strong adhesive strength and superior bioactive property. The adhesion strategy that combined a particle packing theory and an English ivy mechanism was firstly applied to the intervertebral disc repair field, which benefited AF seal. The modified method of incorporating polyphenols was utilized to confer with ROS-scavenging capacity, ECM metabolism regulation ability and anti-inflammatory property, which promoted NP augmentation. Thus, PPU-glue attained the

* Corresponding authors at: Department of Histology and Embryology, NMPA Key Laboratory for Safety Evaluation of Cosmetics, School of Basic Medical Sciences, Guangdong Provincial Key Laboratory of Bone and Joint Degeneration Diseases, The Third Affiliated Hospital of Southern Medical University, Southern Medical University, Guangzhou 510515, PR China.
*E-mail addresses:* taomeihan92@163.com (M. Tao), luzhihui@ciac.ac.cn (Z. Lu), jsguo4127@smu.edu.cn, guojinshan@ciac.ac.cn (J. Guo).

https://doi.org/10.1016/j.actbio.2024.09.038

synergy effect for post discectomy therapy, and the design principle could be universally expanded to the bioadhesives for other surgical uses.



## 1. Introduction

Intervertebral disc (IVD) herniation is a prevalent spinal condition, which is a leading cause of low back pain that affects about 60 %–80 % of all individuals during their lifetimes [1–3]. Degenerated discs are generally considered as the main source of pain, since annulus fibrosus (AF) defect often leads to nucleus pulposus (NP) extrusion, thus causing nerve compression and injury [4–7]. Discectomy is the established surgical procedure for alleviating low back pain caused by IVD herniation. In this procedure, the extruded NP tissue is removed to decompress the affected nerve tissue [8]. However, this procedure neither can suppress NP degeneration nor seal AF defect, rendering it only as a palliative treatment to alleviate clinical symptoms [9,10]. There still remains progressive structural failure, namely the residual NP tissue may protrude through the persistent AF defect [11], which is likely to exacerbate IVD degeneration. Hence, recurrent herniation (re-herniation) often occurs (with reported rates up to 25 %), which is a major reason for reoperation following primary discectomy [12–15]. Although re-herniation is an acknowledged problem, there is still no established method for the therapy of AF defect and NP degeneration after discectomy at present.

Various biomaterials have been designed for the repair of AF, NP and total IVD. For instance, an injectable and photocurable TGF-$\beta$1-supplemented decellularized annulus fibrosus matrix hydrogel was developed to seal AF defect [16]. Fucoidan-loaded nanofibrous scaffolds were also fabricated by electrospinning for AF repair [17]. Previous studies have reported that injectable hydrogel microspheres could regulate NP degenerative microenvironment, such as overactive inflammation and extracellular matrix (ECM) metabolism imbalance [18,19]. Besides, a bioinspired tissue-engineered IVD was constructed for total disc replacement targeting late-stage IVD degeneration [20]. Undoubtedly, these biomaterials have exhibited remarkable repair effecacy in the corresponding disease models. However, considering the anatomical structure and physiological status of the IVD after discectomy, biomaterials that can seal AF defect and suppress NP degeneration are urgently needed [21–23].

Bioadhesives are widely applied for tissue wound healing, and commonly classified as adhesives, hemostats and sealants in terms of function [24,25]. Given the practical application for post discectomy therapy, there is a need for an injectable bioadhesive that can act both as a tissue adhesive and a sealant [21]. As an adhesive, it can adhere to the native fibrocartilage and minimize the likelihood of implant shedding. Simultaneously, as a sealant, it can seal AF defect and prevent IVD re-herniation. Recently, an alginate-based tissue-mimetic hybrid bioadhesive was developed for IVD repair, serving as both a NP glue and an AF sealant [26]. Besides, a glue composed by two parts, oxidized and methacrylated glycosaminoglycan and fibronectin-conjugated fibrin plus poly (ethylene glycol) diacrylate (PEGDA), was designed for AF repair to provide tissue adhesion and stress buffer separately [27]. Remarkably, a super-strong English ivy-inspired aqueous glue was reported and applied for dura seal and repair [28]. Inspired by various biological, chemical and physical adhesion strategies employed by animals and plants, biomimetic bioadhesives could produce strong adhesion to tissues [28,29]. For physical adhesion strategy, previous studies have clarified that English ivy can secrete spherical glycoprotein nanoparticles, which can permeate into the crevices of vertical walls to form mechanical interlock after film formation, meanwhile, the film is further strengthened by calcium ion-driven electrostatic interaction [30]. Certainly, besides the outstanding adhesion property, bioactivity should be taken into account [31], because IVD is the largest avascular organ with poor self-healing property in humans [32]. As reported, oxidative stress may be a "chief culprit" in degenerated discs [33], which is usually triggered by reactive oxygen species (ROS) overproduction [33,34]. Nevertheless, current studied and existing commercially bioadhesives generally lack ROS-scavenging capacity. Thus a bioadhesive that possesses certain adhesive strength and bioactivity should be an ideal candidate for post discectomy therapy.

Polyphenols have become increasingly attractive to biomaterials with good anti-oxidant and anti-inflammatory properties [34–36]. Among them, tannic acid (TA) and curcumin (Cur) have showed their protective effects in the IVD therapy field, mainly aim at NP degenerated microenvironments such as ECM metabolism imbalance [37–41]. Herein, inspired by the nanoparticle permeation, mechanically interlock and electrostatic interaction strategies employed by English ivy, cationic waterborne polyurethane nanodispersions ($WPU^+$) with larger particle sizes and anionic waterborne polyurethane nanodispersions ($WPU^-$) with smaller particle sizes were synthesized and nanodispered in water by self-emulsification. TA and Cur were also introduced via physical mixture and chemical bonding separately to prepare TA/$WPU^+$ (physical mixing) and Cur-$WPU^-$ (Cur chemically integrated in polymer backbone). Then a polyphenol-modified waterborne polyurethane bioadhesive (PPU-glue) was developed by simply mixing TA/$WPU^+$ and Cur-$WPU^-$ with a volume ratio of 1/1. Benefiting from the English ivy adhesion strategy and particle packing theory that the mismatched particle sizes and the electrostatic interaction between cationic and ionic nanodispersions will enhance particle packing density [28], PPU-glues exhibited strong adhesive strength conduciving to seal AF defect. The incorporation of polyphenols conferred PPU-glues with superior ROS-scavenging capacity, ECM metabolism regulation ability and anti-inflammatory property, which are beneficial to suppress NP degeneration. The swelling behavior, degradation and polyphenols release profiles, tissue adhesion strength, biocompatibility and bioactivity were thoroughly investigated, and therapeutic effecacy to seal AF defect and ameliorate nucleus pulposus (NP) degeneration after discectomy was also evaluated on a degenerated rat model via radiological, histological and biomechanical approaches.

## 2. Materials and methods

### 2.1. Materials

Polycaprolactone diol (PCL diol, Mw = 1000 Da) was obtained from DAICE. Isophorone diisocyanate (IPDI), 1, 4-butanediol (BDO), Cur and TA were purchased from Macklin. Dimethylol propionic acid (DMPA) was gained from Shanghai yuanye Bio-Technology Co., Ltd. N-methyl diethanolamine (MDEA) was acquired from Meryer. Ethylenediamine monohydrate (EDA·$H_2O$) and 2-dimethylaminoethanol (DMAE) were provided by Aladdin.

### 2.2. Synthesis and characterizations of WPU nanodispersions

For the synthesis of WPU$^-$, PCL was added in a dried four-necked, round-bottomed flask, then was stirred and removed water under vacuum at 100 ºC for 3 h. Subsequently, the temperature was reduced to 60 ºC, then IPDI in dried acetone was added and the reaction was conducted at 60 ºC under nitrogen atmosphere for 1 h. Next, DMPA in acetone and BDO were added at 60 ºC and the reaction was continued with stirring for 4 h. Acetone was refluxed by a graham condenser and was supplied when the system viscosity increased. Afterwards, DMAE was added to neutralize the side chain carboxyl groups from DMPA (the neutralization degree [$N_{DMAE}$ /$N_{DMPA}$ ×100 %, N means molar amount] close to 100 %) at 60 ºC for 30 min. After reducing the temperature to 30 ºC, the reaction mixture was transferred to a beaker. EDA in deionized water was poured into the system with stirring at 3000 rpm for 10 min using an emulsifying machine (IKA T18 Digital Packag, Germany) to obtain WPU$^-$ nanodispersion. For Cur-WPU$^-$, the amounts of DMPA and BDO were adjusted, and Cur in acetone was added into the reaction system after chain extension by DMPA and BDO, and the reaction was continued for another 3 h at 60 ºC. For WPU$^+$, MDEA was used to replace DMPA being used in WPU$^-$, and acetic acid (HAc) was used as counterion containing compound. For WPU$^-$, the molar ratio of PCL/IPDI/DMPA/BDO/EDA was 4:9:2.9:1.0:0.67. For Cur-WPU$^-$, the molar ratio of PCL/IPDI/DMPA/BDO/Cur/EDA was 4:9:2.84:1.0:0.06:0.67. And for WPU$^+$, the molar ratio of PCL/IPDI/MDEA/BDO was 4.17:13.5:5.87:3.11.

The particle sizes and zeta potentials of WPU$^+$, WPU$^-$ and Cur-WPU$^-$ were determined by dynamic light scattering (DLS) (Malvern, Zetasizer Advance Range, UK). The solid contents of WPU$^+$, WPU$^-$ and Cur-WPU$^-$ were measured by mass change before and after vacuum freeze-drying. The chemical structures of WPU$^+$, WPU$^-$, Cur-WPU$^-$, IPDI and Cur were characterized using an attenuated total reflectance Fourier transform infrared (ATR-FTIR) spectrometer (Thermo Fisher Scientific Nicolet iS10, America).

The macroscopical migration of WPU$^-$, Cur-WPU$^-$ (chemical modification) and Cur/WPU$^-$ (physical blend) was observed to further confirm whether Cur was chemically introduced to Cur-WPU$^-$ or not. Briefly, they were diluted by deionized water and equivalent chloroform were added in the bottom, then were stirred for 12 h. Finally, the color and transparency of bottom layer liquid was recorded.

### 2.3. Preparation of bioadhesives (PPU-glue)

PPU-glue was composed of anionic nanodispersions and cationic nanodispersions. There were 4 kinds of combinations used in the study as follows: (i) WPU$^-$ and WPU$^+$ were mixed at a volume ratio of 1:1 to obtain a polyurethane bioadhesive (namely PU); (ii) TA solution (10 wt %) was added to WPU$^+$ at a volume ratio of 0.1:1 (TA/WPU$^+$), and then WPU$^-$ and TA/WPU$^+$ were mixed at a volume ratio of 1:1 (PUT); (iii) Cur-WPU$^-$ and WPU$^+$ were mixed at a volume ratio of 1:1 (PUC); (iv) Similar to PUT, Cur-WPU$^-$ and TA/WPU$^+$ were mixed at a volume ratio of 1:1 (PUCT).

### 2.4. Characterizations of PPU-glue

The swelling ratios of PPU-glues were measured by immersing dried PPU-glue films in deionized (DI) water until fully swollen. The weight ratios of the swollen parts and the dry films were calculated to be the swelling ratios (in percentage). The degradation property of PPU-glue was investigated by recording the mass loss of dried PPU-glue films in PBS at 37 ºC for 12 weeks, and PBS was changed every two weeks. The cumulative release profiles of TA and Cur were detected by UV-vis spectrophotometry (Shimadzu UV-2550, Japan). Briefly, freeze-dried samples were immersed in PBS at 37 ºC. The supernatant liquid was collected at pre-determined time points (2, 4, 6, 8, 10, 14, 20, 28 and 30 d), and the absorbances of TA and Cur were separately recorded at 278 nm and 426 nm. Three specimens were set in each group, and the results were averaged.

To evaluate the adhesion property, we conducted lap shear tests and burst pressure tests according to ASTM F2255-05 and ASTM F2392-04 respectively. For lap shear tests, the porcine skin was cut into rectangle strips after removing the fat of inner layer. 200 µL anionic dispersions and 200 µL cationic dispersions were applied to two slides separately. Subsequently, the two slides were overlapped with a bonding area of 10 × 10 mm$^2$, and were compressed to form a compact adhesive layer. The samples were set in the Instron machine (34TM-10, USA) and stretched until the adhered procine skins were seperated from each other. The tensile rate was 5 mm min$^{-1}$. The lap shear strength was calculated as the maximum load / the bonding area. For burst pressure tests, a piece of porcine skin was made a 3-mm-diameter circular defect in the middle. Afterwards, 50 µL anionic dispersions and 50 µL cationic dispersions were applied and mixed instantly, then formed a plug to seal the defect. The substrate was sandwiched between two stainless steel discs, one of them was linked with a syringe by pipes. Force was applied to the syringe plunger and the rate was 5 mm min$^{-1}$. The peak pressure was measured and recorded using the Instron 34TM-10. The burst pressure strength was calculated as the peak pressure / the sectional area of syringe. The fibrin glue, composed of 80 mg mL$^{-1}$ fibrinogen and 500 units mL$^{-1}$ thrombin, was used as control. Eight specimens were set in each group and the results were averaged.

### 2.5. ROS-scavenging capacity of PPU-glue

To examine ROS-scavenging capacity of PPU-glue, 2,2-diphenyl-1-picrylhydrazyl (DPPH, D4313, TCI) assay and 2,2′-azino-bis-3-ethylbenzothiazoline-6-sulfonic acid (ABTS, A9941-5TAB, Sigma-Aldrich) assay were conducted. For DPPH assay, 3 mL 100 µM DPPH solution was incubated with 30 mg dried PPU-glue for 45 min under dark. The scavenging capacity of PPU-glue was observed by UV-vis spectrophotometer (Shimadzu UV-2550, Japan) at the wavelength of 517 nm. The blank control was the DPPH solution without any treatment. For ABTS assay, 3 mL 100 µM ABTS solution was incubated with 75 mg dried sample for 80 min under dark. The blank control was the ABTS solution without any treatment. The scavenging capacity was detected at 734 nm. Four specimens were tested in each group and the results were averaged.

To detect intracellular ROS-scavenging capacity of PPU-glue, a ROS probe (S0033S, Beyotime) was used. NP cells (NPCs) were seeded in 24-well plates ($3\times10^4$ cells well$^{-1}$), then 50 µM Tert-butyl hydroperoxide (TBHP) and PPU-glue film were used to treat NPCs for 24 h. Later, the NPCs were incubated with 2,7-dichlorodihydrofluorescein diacetate (DCFH-DA) solution away from light for 60 min. Last, the NPCs were imaged by a fluorescence microscope (LEICA DM4000 B/DF C425, Germany). The untreated NPCs was set as the negative control, and the positive control group was the only TBHP-stimulated NPCs. Four specimens were set in each group and at least 3 random areas were selected (100× magnification).

### 2.6. In vitro *cytotoxicity evaluation*

The NPCs were isolated from 5-week-old male Sprague-Dawley (SD) rats by digestion with 0.2 % type II collagenase for 4 h. The resulting NPCs suspension was obtained by a 70 µm filter. After centrifugation, the precipitate was re-suspended in DMEM/F12

medium containing 12 % fetal bovine serum. The NPCs of the third to fifth passage were used in the next cell experiments.

To access the cytotoxicity after medium extract treatment or PPU-glue co-culture, CCK-8 assay (BS350B, Biosharp) was performed. For medium extract treatment, 1 g dried sample was immersed in 10 mL medium for 24 h at 37 ºC. The concentration of medium extract was diluted to 1×, 10× and 100×. The NPCs were seeded in 96-well plates ($5\times10^3$ cells well$^{-1}$) for 24 h and incubated with medium extract of different dilutions for another 24 h. For PPU-glue co-culture, the NPCs were seeded in 24-well plates ($3\times10^4$ cells well$^{-1}$) for 24 h, 10 mg dried sample was added with forceps, and they were cultured together for another 24 h and 72 h. The untreated NPCs were used as control. The absorbance at 450 nm was measured by microplate reader (Bio-Tek, USA). At least five specimens were set in each group.

To evaluate the viability after PPU-glue co-culture, Live/Dead staining assay was conducted. Briefly, the NPCs were manipulated in 24-well plates ($3\times10^4$ cells well$^{-1}$) following the co-culture procedure as described above. Afterwards, 300 µL Live/Dead dye liquor was used to treat the NPCs for 20 min. The images were captured by the fluorescence microscope (LEICA DM4000 B/DF C425, Germany) and three random areas were selected (100× magnification). Four specimens were set in each group.

### 2.7. In vitro *PPU-glue treatment of degenerated NPCs*

To generate the oxidative stress environment and establish a degenerated IVD model *in vitro*, 50 µM TBHP was used to stimulate the NPCs for 24 h as described previously [37,38] followed by being treated with PPU-glue for another 48 h. qRT-PCR was performed to analyze the gene expression associated with ECM metabolism, including collagen type II (Col-II), aggrecan (Acan), matrix metalloproteinase-13 (Mmp-13), a disintegrin and metalloproteinase with thrombospondin motifs-4 (Adamts-4) and tissue inhibitor of matrix metalloproteinase-1 (Timp-1). The NPCs were plated in 6-well plates ($1\times10^5$ cells well$^{-1}$), and five groups were assigned: (i) no treatment (blank control group), (ii) TBHP stimulation (TBHP group), (iii) TBHP stimulation and PU treatment (PU group), (iv) TBHP stimulation and PUT treatment (PUT group), (v) TBHP stimulation and PUCT treatment (PUCT group). RNA was extracted using TRIzol reagent and converted into first-strand cDNA. The genes and the primer sequences (Sangon Biotech, China) were listed in Table S1. The relative mRNA expression of each gene was normalized to the housekeeping gene Actin and analyzed using the $2^{-\Delta\Delta Ct}$ method. Four specimens were set in each group.

Immunofluorescence staining was used to detect the protein expression of ACAN and COL-II, representing ECM metabolism. Briefly, the NPCs were treated as described above. The NPCs were fixed in 4 % paraformaldehyde, permeabilized with 0.3 % Triton-X100, and blocked with 5 % bovine serum albumin. Then they were incubated with ACAN (Rabbit, 13880-1-AP, 1:100) and COL-II (Rabbit, 28459-1-AP, 1:100) antibodies at 4 ºC overnight. Later, the NPCs were incubated with a fluorescent antibody (Goat anti-Rabbit IgG, A23420, 1:200). Then the NPCs were incubated with DAPI solution (P0131, Beyotime, China). The images were observed and photographed using the upright fluorescence microscope (LEICA DM4000 B/DF C500, Germany) and 3 random areas were selected (400× magnification). There were four parallel specimens of each group.

### 2.8. In vivo *PPU-glue treatment of degenerated rat caudal discs*

A total of 60 male SD rats aged 10 weeks were purchased from the Medical Animal Experiment Center of Southern Medical University. All animal experiments were in compliance with the Animal Experimental Committee of Institute of Biological and Medical Engineering, Guangdong Academy of Sciences (Approval No. 2023061). Five groups were assigned in total: (i) no puncture (normal group), (ii) puncture and PBS injection (defect group), (iii) puncture and PU treatment (PU group), (iv) puncture and PUT treatment (PUT group), (v) puncture and PUCT treatment (PUCT group).

To evaluate the therapeutic effects of PPU-glue, a needle-puncture model was conducted to induce IVD degeneration. After anesthesia, a 2-cm-longitudinal incision was made on rat caudal dorsal skin, and the Co7/8 was punctured in the center of disc with a 21G needle. After rotating 360°, the needle held in place for 30 s. The puncture resulted in a full-thickness AF defect measuring approximately 0.80 mm in diameter and 1.40 mm in depth, with minimal NP damage. Subsequently, 3 µL anionic dispersions and 3 µL cationic dispersions of PPU-glue were injected into the newly created AF defect. Finally, all the rats were euthanized using pentobarbital sodium (200 mg/kg) at 4 or 8 weeks after surgery, and disc samples were collected for analysis.

#### 2.8.1. Radiological evaluation

Radiologically, X-Ray and MRI were used to evaluate disc degeneration after surgery for 4 and 8 weeks. X-Ray images were acquired using the radiography machine (Bruker FX Pro, USA). The disc height index (DHI) was calculated by twice the sum of the anterior, middle and posterior edge heights of the intervertebral space / the sum of the anterior, middle, and posterior heights of the adjacent vertebral bodiesas as previously reported [16]. At each time point, the DHI % was quantified as the DHI in the treatment group / the DHI in the normal group × 100. The T2-weighted section images (TR = 4000 ms, TE = 56 ms, slice thickness = 0.8 mm, plane resolution = 300 × 180) were captured with the 7.0T MRI scanner (Bruker PharmaScan70/16 US, USA). The images were classified as grades I to IV in accordance with Pfirrmann grading system (Table S2) by two well-trained graders, and they were blinded to the treatment groups. Four specimens were assessed in each group, and the results were averaged.

#### 2.8.2. Histological evaluation

Gross appearance assessment was conducted after surgery for 4 and 8 weeks. Briefly, the discs were fixed with 4 % paraformaldehyde, and decalcified in 10 % EDTA. Thompson score system (Table S3) was used to assess disc degeneration. The images were observed and photographed using the stereo microscope (SOPTOP SZX12, China). Four specimens were set in each group.

Hematoxylin and Eosin (H&E) staining and Safranin O-fast Green (S&O) staining were also conducted to preliminarily assess the theraputic efficacy of PPU-glue through observing IVD morphology and structure as well as collagen deposition and composition. The discs were harvested and fixed with 4 % paraformaldehyde at 4 and 8 weeks after surgery. After decalcification and dehydration, all the discs were embedded in paraffin, sliced to a thickness of 5 µm and stained by dyes. The histological grading system was divided into 5 major categories in accordance with JOR Spine/ORS Spine Section grading scale (Table S4). Two well-trained graders were blinded to the treatment groups. Furthermore, immunohistochemical staining was performed as previously reported [42] to assess the expression of ACAN (13880-1-AP, proteintech, 1:400), COL-II (28459-1-AP, proteintech, 1:1600) and MMP-13 (GB11247-100, Servicebio, 1:400). The slices were incubated with primary antibodies overnight at 4 ºC, followed by being treated with HRP conjugated goat anti-Rabbit IgG (1:200, Beyotime, Shanghai, China) for 2 h. Finally, the slices were visualized with DAB (Sangon Biotech, Shanghai, China) for 30 s and counterstained with hematoxylin. The images were observed and photographed under the upright microscope (LEICA DM4000 B/DF C500, Germany). Four specimens were studied in each group.

*2.8.3. In vivo organotoxicity evaluation*

To access the organotoxicity after surgery for 8 weeks, the major organs of the treated rats including heart, liver, spleen, lung and kidney were harvested, fixed with 4 % paraformaldehyde, embedded in paraffin, and the pathological slides were assessed with H&E staining. The images were evaluated by two well-trained graders, and they were blinded to the treatment groups. Four specimens were set in each group.

*2.8.4. Biomechanical tests*

The uniaxial compression test was performed on the rat tail discs after surgery for 8 weeks. The discs were collected and stored in PBS at 4 ºC. Before testing, the discs were conditioned for 1 h ± 15 min in PBS at room temperature. The test was programmed at a compression rate of 0.2 mm $min^{-1}$ until the displacement reached 10 % of the height of the IVD. Measurements of the IVD height and diameter were taken using a vernier caliper. The stress was calculated as the force / the area of IVD, and the strain was calculated as the displacement / the height of IVD. The stress-strain curve was used to quantify compression modulus from 0 to 10 % strain according to previous studies [17]. Four specimens were measured in each group and the results were averaged.

Futhermore, an *in vitro* ramp-to-failure test was conducted on bovine tail discs. The discs were compressed on a 5° inclined foundation at a fixed rate of 2 mm $min^{-1}$. The stress was defined as the force / the cross-sectional area of IVD. The failure strength was recorded during extrusion failure or disc subsidence as reported [26]. Three specimens were set in each group and the results were averaged.

*2.9. Statistical analysis*

All statistical data shown were mean ± standard deviation (SD) of at least three independent repetitions in each group. Statistical analyses were performed using ordinary one-way ANOVA with Tukey's multiple comparisons test (GraphPad Prism 8.0 software). The difference is considered statistically significant if $p$ is less than 0.05. $^{*}p < 0.05$, $^{**}p < 0.01$, $^{***}p < 0.001$, $^{****}p < 0.0001$. $p > 0.05$ is considered not significant (ns).

## 3. Results

*3.1. Synthesis and characterizations of nanodispersions*

As shown in Fig. 1A, WPUs were synthesized by the reaction of PCL diol and IPDI, followed by chain extension with small molecular diol and cat/an-ionizable diol, and finally dispersion in water via self-emulsification after being treated with counterion containing compound. Briefly, PCL diol and IPDI were the main reactants, BDO and EDA were the neutral chain extenders. For $WPU^{+}$, MDEA was the cationic extender. For $WPU^{-}$, DMPA was the anionic extender. TA and Cur were introduced to prepare $TA/WPU^{+}$ and $Cur\text{-}WPU^{-}$ via simple mixture and chemical bonding, respectively.

As mentioned above, the mismatched particle sizes of $WPU^{+}$ and $WPU^{-}$ enhanced particle packing and interfusion, and the contrary ions of $WPU^{+}$ and $WPU^{-}$ caused electrostatic interaction [28]. Accordingly, $WPU^{+}$ with large particle sizes and $WPU^{-}$ and $Cur\text{-}WPU^{-}$ with small particle sizes were synthesized, the particle sizes and zeta potentials were characterized by dynamic light scattering (DLS, Zetasizer). As shown in Fig. 1B, the average particle sizes of $WPU^{+}$, $WPU^{-}$ and $Cur\text{-}WPU^{-}$ were 147.40 ± 1.54 nm, 33.08 ± 0.46 nm and 50.21 ± 0.65 nm, respectively. The average zeta potentials of $WPU^{+}$, $WPU^{-}$ and $Cur\text{-}WPU^{-}$ were 32.68 ± 0.42 mV, -38.55 ± 2.14 mV and -9.97 ± 0.64 mV, respectively (Fig. 1C). The solid contents of $WPU^{+}$, $WPU^{-}$ and $Cur\text{-}WPU^{-}$ were in the range of 30-40 wt % (Fig. 1D).

The FTIR spectra (Fig. 1E) of $WPU^{+}$, $WPU^{-}$ and $Cur\text{-}WPU^{-}$ display the shoulder peaks of the imido (-NH-) in the urethane bonds at 3360 $cm^{-1}$. The peaks around 2945 $cm^{-1}$ and 2865 $cm^{-1}$ are separately assigned to symmetric and asymmetric methylene (-$CH_2$-) stretching vibration absorption peak. The peaks around 1724 $cm^{-1}$ are assigned to the carbonyl groups (C=O). There was no remaining isocyanate group at 2243 $cm^{-1}$ derived from IPDI in all the WPUs, indicating successful synthesis. Thus, the above results confirm the formation of urethane bonds. In addition, the spectrum (Fig. S1A) of Cur shows a broad peak at 3507 $cm^{-1}$ assigned to hydroxy association, which decreased signifcantly in $Cur\text{-}WPU^{-}$. It might because the hydroxy on Cur could react with the isocyanate of prepolymer. The ultraviolet visible (UV-vis) absorption spectra (Fig. S1B) shows a characteristic absorption peak around 426 nm from Cur in $Cur\text{-}WPU^{-}$, while there was no peak in $WPU^{-}$, indicating Cur was successfully introduced to $Cur\text{-}WPU^{-}$.

Additionally, we observed the macroscopical migration of $WPU^{-}$, $Cur\text{-}WPU^{-}$ (chemical modification) and $Cur/WPU^{-}$ (physical blend) in aqueous phase and organic phase. As shown in Fig. S1C, there was nearly colorless and transparent liquid in the bottom layer of $WPU^{-}$ and $Cur\text{-}WPU^{-}$ after stirring for 12 h. However, the bottom layer liquid turned yellow visibly in $Cur/WPU^{-}$, suggesting free Cur was extracted by chloroform. This further confirms that Cur was chemically introduced to the polymer of $Cur\text{-}WPU^{-}$.

*3.2. Preparation and characterizations of bioadhesives*

Waterborne polyurethane bioadhesives were basically composed of $WPU^{+}$ and $WPU^{-}$. There were 4 kinds of single component, including $WPU^{+}$, $TA/WPU^{+}$, $WPU^{-}$ and $Cur\text{-}WPU^{-}$. Thus 4 combinations were arranged, including $WPU^{+}/WPU^{-}$ (namely PU), $TA/WPU^{+}/WPU^{-}$ (PUT), $WPU^{+}/Cur\text{-}WPU^{-}$ (PUC) and $TA/WPU^{+}/Cur\text{-}WPU^{-}$ (PUCT). The macroscopical images of single component and composite gelation are shown in Fig. S2. All the formulations exhibit fast-gelation (<10 s) as shown in Fig. S3, which is deemed caused by fast electrostatic interaction as well as particle packing and interfusion (Fig. 2A).

As shown in Fig. 2B, the swelling ratios of all the samples were lower than 15 % and 35 % after soaking in PBS for 1 day and 30 days, respectively. There was no significant difference between groups at the same time points. The above results show the minimal swelling behavior of PPU-glue, which could avoid the over-expansion problem that commonly occurs in hydrogel-based adhesives. As shown in Fig. 2C, the degradation rates increased after the introduction of TA and further increased by incorparating Cur, while there was nearly no degradation in PU within 12 weeks.

The cumulative release profiles of Cur and TA are separately shown in Fig. 2D and 2E. The release of polyphenols continued and reached a plateau after approximately 14 days. It could be noted that TA release concentration of PUCT was higher than that of PUT at the same time points, while Cur release curves of PUCT and PUC were almost identical, suggesting that physical mixture was looser than chemical bonding in this study. Collectively, polyphenols could promote the dissociation of PPU-glue, mainly caused by TA of physical mixture and partially caused by Cur of chemical bonding.

*3.3. Adhesion property of PPU-glue*

As reported in previous literature, ASTM F2255-05 and ASTM F2392-04 are the most commonly used standards to evaluate the adhesion property *in vitro* for tissue adhesives and sealants in AF repair [21]. Since NP pressurization induced a radial outward force on AF, lap shear tests and burst pressure tests were conducted, given the direction of applied loads with respect to the bioadhesives.

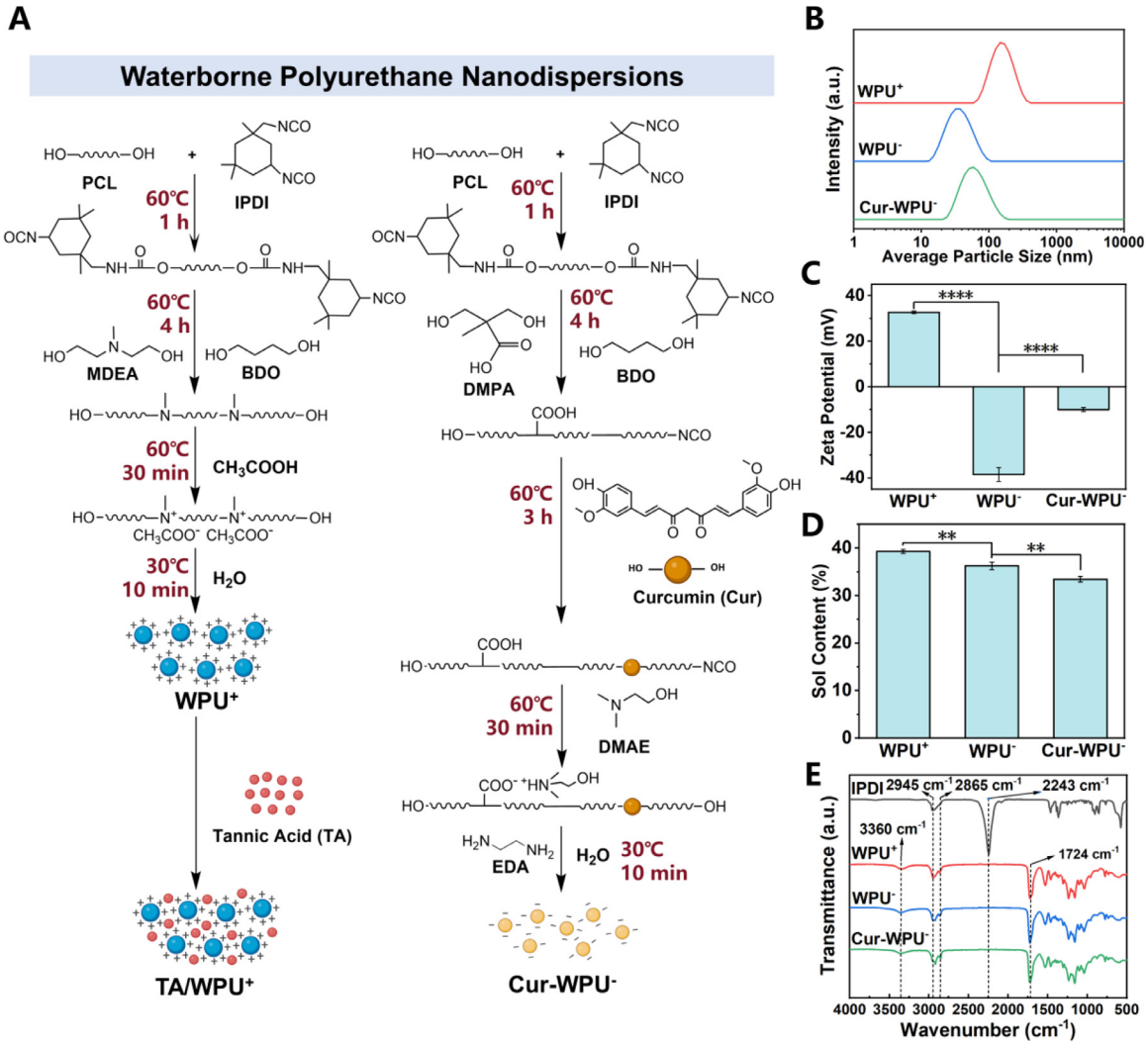


**Fig. 1. Synthesis and characterizations of WPU nanodispersions:** (A) synthetic routes of TA/WPU$^+$ and Cur-WPU$^-$; (B) size distribution, (C) zeta potentials and (D) sol contents of WPU$^+$, WPU$^-$ and Cur-WPU$^-$; (E) FTIR spectra of IPDI, WPU$^+$, WPU$^-$ and Cur-WPU$^-$. ** $p < 0.01$, **** $p < 0.0001$.

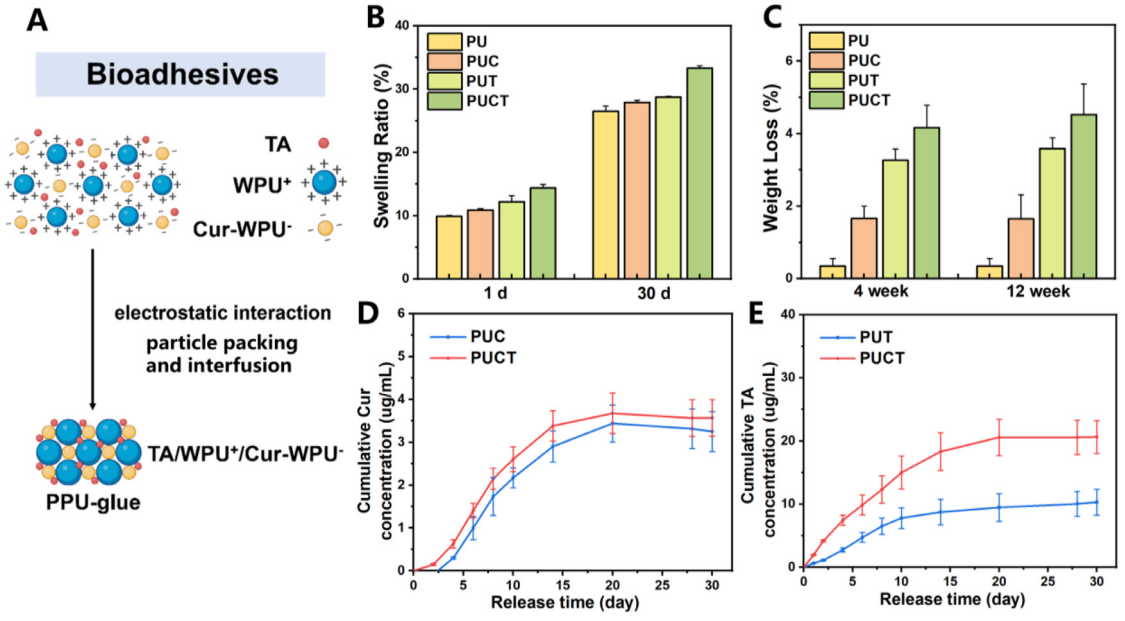


**Fig. 2. Preparation and characterizations of bioadhesives:** (A) preparation process of TA/WPU$^+$/Cur-WPU$^-$ bioadhesive; (B) swelling ratios, (C) degradation rates of bioadhesives at pre-determined time-points; cumulative release curves of (D) curcumin (Cur) and (E) tannic acid (TA).

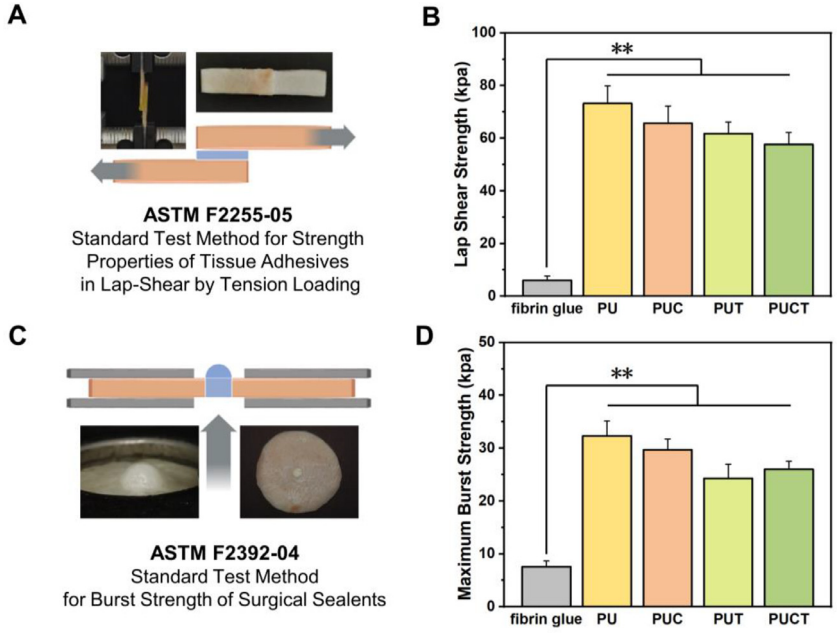


**Fig. 3. Adhesion property of bioadhesives:** (A, B) lap shear test and (C, D) burst pressure test of the bioadhesives against wet porcine skin. $^{**}p < 0.01$.

Fig. 3A shows the schematic diagram of lap shear test and photographs of specimen. The lap shear strengths (Fig. 3B) of PU, PUC, PUT and PUCT were 73.19 ± 6.70 kPa, 65.67 ± 6.50 kPa, 61.75 ± 4.40 kPa and 57.61 ± 4.57 kPa, respectively, all significantly higher than ($p < 0.01$) that of fibrin glue (5.98 ± 1.68 kPa). There was no significant difference between the experiment groups. Fig. 3C shows the schematic diagram of burst pressure test and photographs of specimen. The maximum burst pressures (Fig. 3D) of PU, PUC, PUT and PUCT were 32.34 ± 2.80 kPa, 29.70 ± 2.04 kPa, 24.28 ± 2.69 kPa and 26.00 ± 1.51 kPa, respectively. Similarly, they were all significantly higher ($p < 0.01$) than that of fibrin glue (7.56 ± 1.08 kPa), but they were not significant difference between the experiment groups. Compared with PU, the maximum burst strengths of PUC, PUT and PUCT were marginally lower, PPU-glues still exhibited strong adhesion strengths after introducing polyphenols.

### 3.4. ROS-scavenging capacity of PPU-glue

ROS plays a crucial role in the pathological process of IVD degneration. The activities of excessive ROS production and clearance are connected with the balance between oxidation and antioxidation [43]. The disrupted balance will lead to oxidative stress, which can accelerate the degneration [44]. As reported, polyphenols possess good anti-oxidant ability via providing electrons to reduce the free radicals [45,46]. The ROS-scavenging capacity of PPU-glue was examined using DPPH and ABTS assay. Fig. 4A shows the DPPH solution absorbances of PUC, PUT and PUCT decreased visibly, while the UV-vis curve of PU was almost the same as the blank group. As shown in Fig. 4B, PUT exhibited the significant DPPH scavenging efficiency (71.91 %) at 30 min, which is deemed to be derived from pyrogallol groups of TA. The DPPH scavenging efficiency of PUCT (75.55 %) was further enhanced, and PUC (14.14 %) also showed considerable ROS-scavenging capacity derived from Cur. Along with time extension to 45 min, the DPPH scavenging percentage of PUCT increased to 77.92 % (Fig. 4C and 4D). The ABTS scavenging percentages at 60 min of PU, PUC, PUT and PUCT were 2.72 %, 7.70 %, 64.49 % and 67.49 %, respectively (Fig. 4E and 4F). Thereinto, the ABTS scavenging percentage of PUCT increased to 70.53 % at 80 min (Fig. 4G and 4H). These results indicate that the trends of DPPH and ABTS assay are basically consistent. Therefore, considering their stronger ROS-scavenging capacity, PUT and PUCT were chosen as the representatives of PPU-glues to conduct the following cell and animal experiments.

Furthermore, the intracellular ROS-scavenging capacity was assessed using a ROS probe (DCFH-DA) in the NPCs. Compared to the positive control group, PUT and PUCT groups exhibited lower green fluorescence (Figs. 4I and S4), suggesting that PPU-glue could attenuate TBHP-stimulated oxidative stress effectively in NPCs. Taken together, polyphenols endowed PPU-glue with favorable ROS-scavenging capacity.

### 3.5. Biocompatibility of PPU-glue

As well-known, good biocompatibility is necessary for biomaterials. The results of CCK-8 assay show the cell viabilities were all around 100 % after being treated with medium extract of different dilutions (1×, 10×, 100×) for 24 h (Fig. S5A). Also, the cell viabilities were all higher than 90 % after co-culturing with PPU-glue for 24 h and 72 h (Fig. S5B). Similarly, the Live/Dead staining images (Fig. S5C) show that most NPCs remained alive after co-culturing with PPU-glue for 24 and 72 h. Furthermore, H&E staining was conducted to access the organotoxicity of rats at 8 weeks after surgery. The histological analysis of major organs (Fig. S6), including the heart, liver, spleen, lung and kidney, did not show any tissue damage. In short, PPU-glue possessed good biocompatibility, including negligible cytotoxicity and organotoxicity.

### 3.6. PPU-glue maintained ECM anabolic/catabolic balance in degenerated NPCs

The ECM of NP is mainly composed of ACAN and COL-II, thus they are also serve as the characteristic features in the physiological functions of the normal IVDs. As reported previously, TBHP has been commonly used to degenerate the NPCs, which will result in the reduction of ECM and culminate in the loss of function [38,39,47,48]. It was found that polyphenols could regulate ECM anabolic/catabolic balance in some extent [38,39]. Thus, in this study, we decided to verify the regulation of polyphenols, and

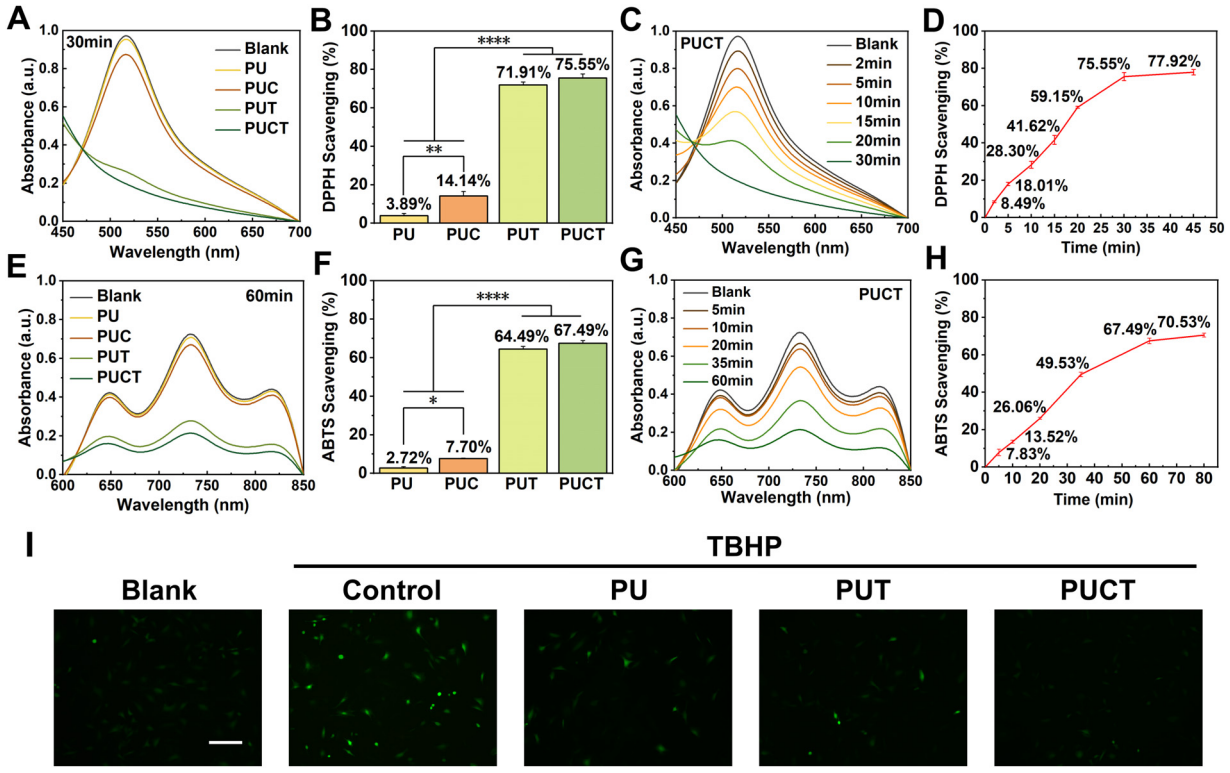


**Fig. 4. ROS-scavenging capacity of PPU-glue:** (A) UV–vis curves and (B) DPPH scavenging percentages after incubating for 30 min; (C) UV–vis curves and (D) dynamic DPPH scavenging percentages of PUCT; (E) UV–vis curves and (F) ABTS scavenging percentages after incubating for 60 min; (G) UV–vis curves and (H) dynamic ABTS scavenging percentages of PUCT; (I) the fluorescent images of ROS overproduction and elimination monitored via DCFH-DA probe in the TBHP-stimulated NPCs after treatment. Scale bar = 200 μm. $^{*}p < 0.05$, $^{**}p < 0.01$, $^{****}p < 0.0001$.

wondered whether PPU-glue had a protective effect on the TBHP-stimulated NPCs or not.

As shown in the immunofluorescence images (Fig. 5A and 5B), the protein expression levels of ACAN and COL-II increased visibly in PUT and PUCT groups, comparing to that of the solely TBHP-stimulated control group (Fig. S7). It preliminarily confirmed that PPU-glue could enhance ECM synthesis in the TBHP-stimulated NPCs.

As shown in the RT-qPCR analysis results (Fig. 5C and 5D), the expression levels of ECM anabolism-related genes, including Acan and Col-II, increased significantly in PUT and PUCT groups, comparing with the control (TBHP) group. The above expression results of protein and mRNA were basically consistent, further confirming that PPU-glue could enhance ECM synthesis in the TBHP-stimulated NPCs. Additionally, the gene expression levels of protease inhibitor Timp-1 also upregulated in the PPU-glue group (Fig. 5E). Conversely, the ECM catabolism-related gene expression levels of Adamts-4 and Mmp-13 significantly downregulated in the PUT and PUCT groups (Fig. 5F and 5G), indicating that PPU-glue could inhibit ECM hyperactive degradation in the TBHP-stimulated NPCs. Specifically, the above results verify that the introduction of TA and Cur could protect the NPCs from TBHP-induced ECM metabolic disturbance. Together, these results prove that polyphenols endowed PPU-glue with the protective ability of maintaining ECM metabolism balance by promoting synthesis and suppressing degradation.

### 3.7. PPU-glue suppressed degeneration in rat caudal discs

The surgery procedures and animal experiments general design are shown in Fig. 6A. Briefly, the rat caudal dorsal skin was incised, making the AF could be observed directly. Then the Co7/8 of rat caudal was punctured with a 21G needle. PPU-glue were injected, then sealed the newly formed AF defect and retained the NP tissue. Later, radiological and histological evaluations were conducted at 4 and 8 weeks after surgery, biomechanical evaluation was also performed at 8 weeks after surgery. The results of animal experiments are described as below.

#### 3.7.1. Radiological evaluation

To verify the therapeutic effects of PPU-glue, X-Ray and MRI were utilized to radiologically evaluate IVD degeneration. X-Ray images show the disc height, and changes in the disc height index (DHI) presenting as DHI %. From X-Ray images (Fig. 6B), it can be seen that a high intervertebral space in the normal group, whereas the space narrowed visibly in the defect group. All the treatment groups presented the inhibition of the disc height loss to different degrees. Likewise, the quantitative analysis of X-ray images (Fig. 6C) suggests that the DHI % of the treatment groups significantly increased comparing to the defect group, particularly in PUT and PUCT groups. Besides, the values of DHI % of PUCT group at week 4 and 8 were nearly the same, implying that PPU-glue could maintain the disc height effectively and enduringly. MRI images reflect the nucleus pulposus water content based on T2-weighted signals, and the degeneration grades were classified by Pfirrmann grading system. From MRI images (Fig. 6D), the signals markedly decreased and even lost in the defect group, while the hyperintense signals well displayed in the normal group. It could be seen that all the treatment groups suppressed the signal loss to certain extent, including PU group. Among the treatment groups, the signals of PUCT group manifested the least loss at 4 and 8 weeks. In other words, PPU-glue could retain the NP tissue, with PUCT group the best, indicating that PPU-glue could seal AF defect successfully. Notably, the loss of signals could be observed along the puncture directions, which were marked by white arrows. The qualitative analysis results of MRI grades (Fig. 6E) show a time-

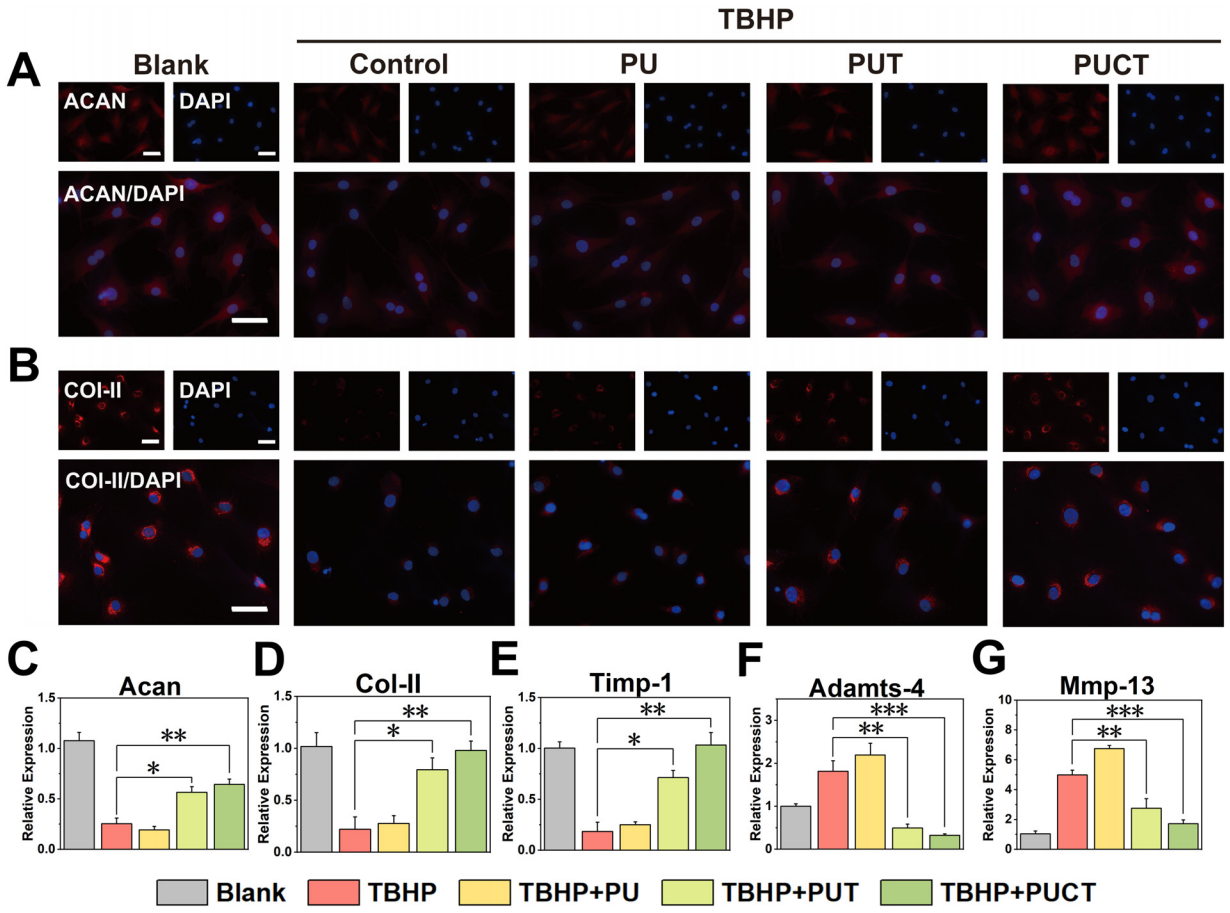


**Fig. 5. Modulation of ECM metabolism balance in the TBHP-stimulated NPCs:** the immunofluorescence images of (A) ACAN and (B) COL-II protein expressions, scale bar = 50 μm; the semi-quantitative analysis of (C) Acan, (D) Col-II, (E) Timp-1, (F) Adamts-4, and (G) Mmp-13 mRNA expressions. $^{*}p < 0.05$, $^{**}p < 0.01$, $^{***}p < 0.001$.

dependent degeneration in all the tested groups, but PPU-glue still achieved remarkable therapeutic effect. In general, the X-Ray and MRI results are basically consistent, suggesting that PPU-glue could seal AF defect and retain NP tissue successfully, thereby maintaining the disc height and delaying the disc degeneration effectively.

### 3.7.2. Histological evaluation

To further prove the protective effects of PPU-glue, histological evaluation was conducted to observe the degenerated discs. The gross appearance images showed the protective effects roughly and directly, and were also classified by Thompson score system. As shown in Fig. 7A, there were serious disruptions of AF structure and devoid of NP tissue in the defect group, but distinct lamellas of AF and intact gelatin of NP in the normal group. Compared with the defect group, the treatment groups showed partial ordered arrangement of AF and retention of NP, espacially in PUT and PUCT groups. From 4 to 8 weeks, the treatment groups presented a slow progression of tissue degeneration. The Thompson score results (Fig. 7B) further demonstrate that PPU-glue could delay IVD continuous deterioration.

The H&E staining images (Fig. 7C) show the morphologies and structures of the IVDs more finely. AF defect and NP absence caused by the needle could be noticed. In the treatment groups, the cartilage endplate was intact, the partial AF was orderly arranged, the reserved NP was clearly demarcated from the surrounding tissue, and the boundary between AF and NP was clear too. Conversely, the defect group exhibited the disordered structures of the collapsed IVDs. The S&O staining images (Fig. 7D) show the content of proteoglycans (orange) and collagen (green). The treatment groups presented that rich proteoglycans were partially replaced by collagen. In other words, NP was gradually replaced by AF. In accordance with the H&E results, the defect group exhibited the entire loss of NP, the complete replacement by AF, and the bone-like tissue eventually replaced the original cartilage-like structure. The histological grade results (Fig. 7E) further illustrate that PPU-glue could maintain the normal morphologies and structures of the IVDs.

The immunohistochemical staining images show the protein expression levels of ACAN, COL-II and MMP-13 in the NP tissue. Similar to the cell experiments, PUT and PUCT groups showed significantly higher contents of ACAN (Fig. 8A and 8B) and COL-II (Fig. 8C and 8D) than that of the defect group. PU group showed matrix reservation as well, which is deemed attributed to the successful AF seal. The results of MMP-13 present the opposite tendency to ACAN and COL-II (Fig. 8E and 8F). It was found that ECM production increased and MMP activity decreased in the treatment groups, indicating that PPU-glue could maintain ECM metabolism balance. Further, Fig. S8 shows that PPU-glue decreased IL-6, IL-1$\beta$ and Tnf-$\alpha$ protein expression levels, suggesting that PPU-glue could suppress NP inflammation *in vivo*.

### 3.7.3. Biomechanical evaluation

To confirm the functional impact of PPU-glue, the uniaxial compression test was performed to evaluate the biomechanical strength recovery. As illustrated in Fig. 9A, the rat discs were used to test. The representative stress-strain curves (Fig. 9B) of the defect group show that the strain increased rapidly during the stress was applied. While, the curves of the treatment groups are rel-

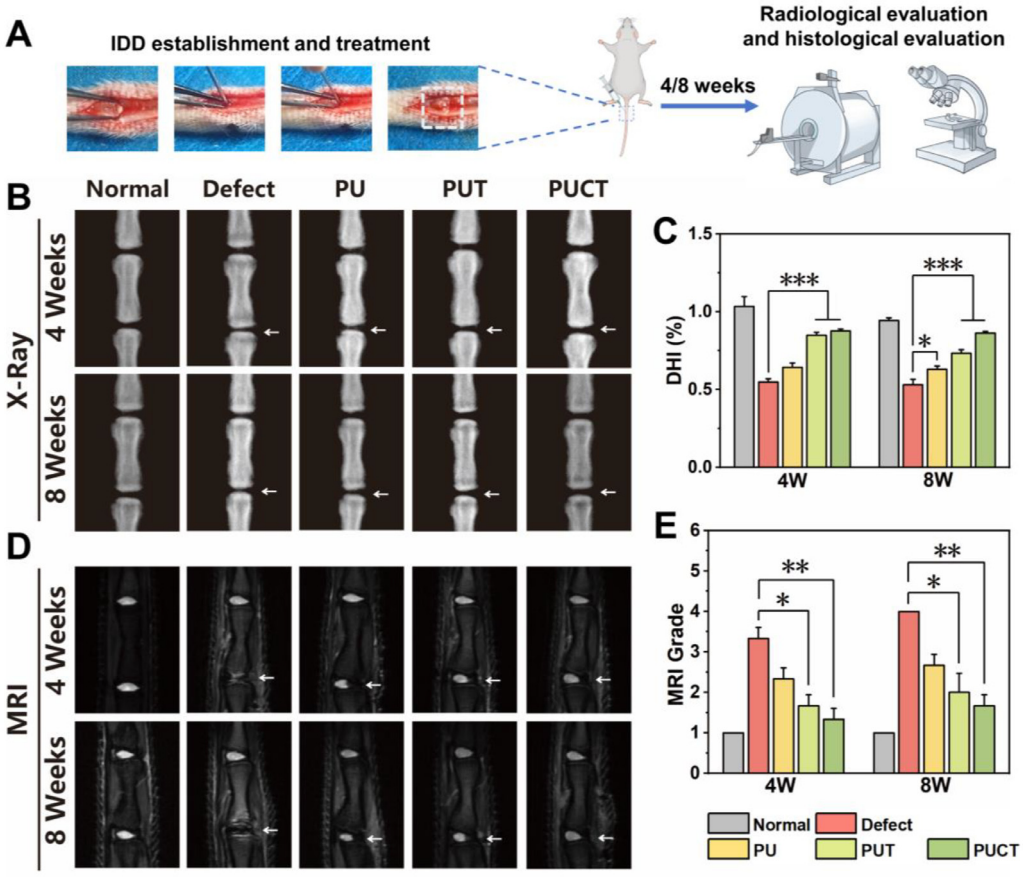


**Fig. 6. Radiological evaluation:** (A) diagram of surgical procedures and design of animal experiments; (B) the images of X-Ray and (C) the changes of DHI at 4 and 8 weeks after surgery; (D) the images of MRI and (E) the changes of Pfirrmann grading scores after surgery for 4 and 8 weeks. The white arrows denote the puncture sites. $^{*}p < 0.05$, $^{**}p < 0.01$, $^{***}p < 0.001$.

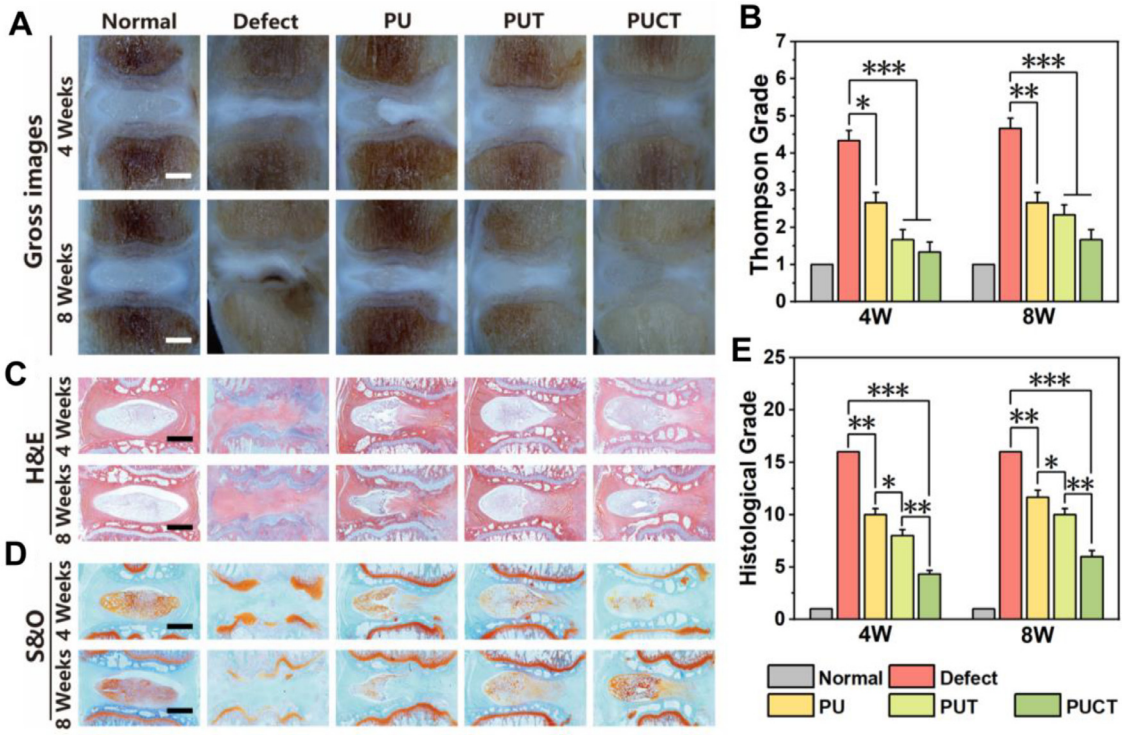


**Fig. 7. Histological evaluation:** (A) the images of gross morphology and (B) the scores of Thompson grading system at 4 and 8 weeks after surgery; the images of (C) H&E and (D) S&O staining, and (E) the scores of histological grading system at 4 and 8 weeks after surgery. Scale bar = 1 mm. $^{*}p < 0.05$, $^{**}p < 0.01$, $^{***}p < 0.001$.

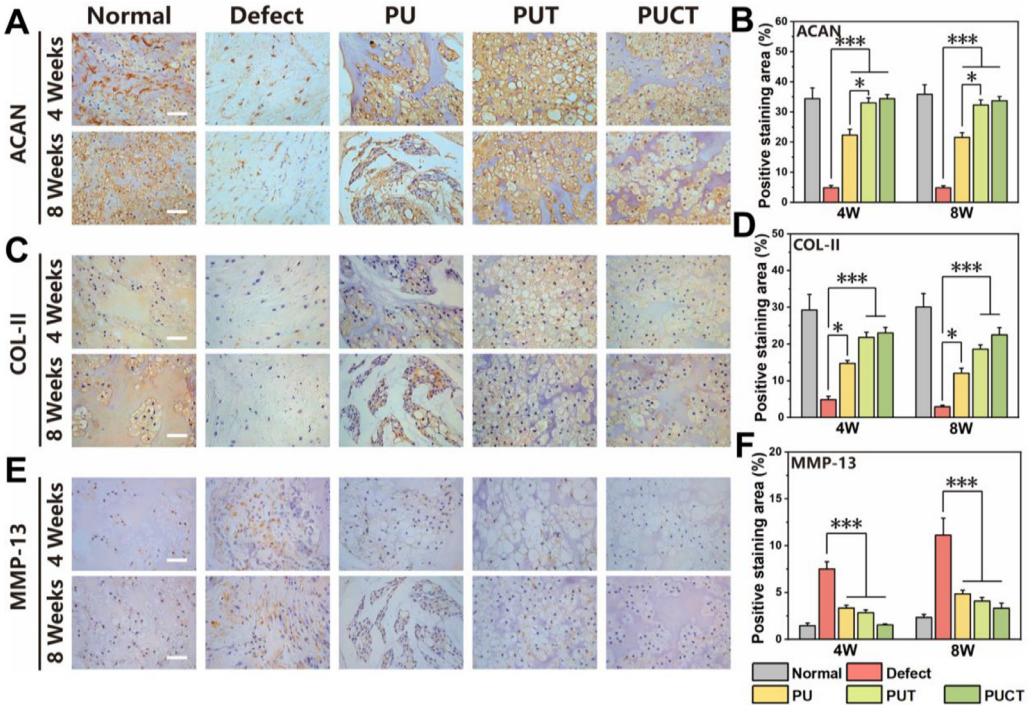


**Fig. 8. Immunohistochemical staining results:** the images and quantitative analysis of (A, B) ACAN, (C, D) COL-II and (E, F) MMP-13. Scale bar = 50 μm. $^{*}p < 0.05$, $^{***}p < 0.001$.

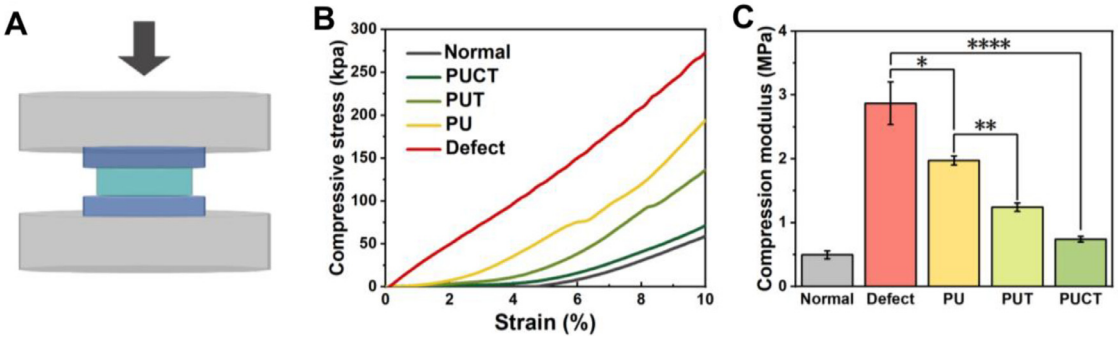


**Fig. 9. Biomechanical evaluation:** (A) diagram of the uniaxial compression tests performed on the rat caudal discs; (B) the representative stress-strain curves; (C) the compression moduli. $^{*}p < 0.05$, $^{**}p < 0.01$, $^{****}p < 0.0001$.

atively flat. The compressive moduli of the treatment groups decreased significantly comparing to the defect group (Fig. 9C). Notably, the curves and compressive moduli of the treatment groups were similiar to the normal group, especially the PUCT group. These results indicate that PPU-glue was conducive to biomechanical function preservation. Further, we conducted the ramp-to-failure tests on the bovine tail discs *in vitro* (Fig. S9A). The representative stress-displacement curve of the normal group shows that the intact bovine disc failed by disc subsidence, and the curves of PUCT group and the defect group exhibit the discs failed by NP or materials extrusion (Fig. S9B). Besides, Fig. S9C shows the failure strength of PUCT group was higher than the defect group, and it is above the physiological upper bound of intradiscal pressure (2.3 MPa).

Overall, the *in vivo* results clarify that PPU-glue could seal the AF defect and retain the NP tissue effectively, and it could maintain the disc height, morphology, structure and ECM metabolism balance, thereby promoting the biological and biomechanical therapy. In brief, PPU-glue had considerable therapeutic effect on degenerated rat caudal discs.

## 4. Discussion

Currently, there are growing concerns about post discectomy therapy. Although some therapy strategies yield good short-term results, long-term prognoses are always unsatisfactory, such as osteophyte formation and endplate damage arising from some mechanical devices [26]. The urgent lack of treatments motivates the flourishing development of biomaterials in the IVD therapy field. Among them, bioadhesives are promising alternatives due to the minimal invasion and superior mechanical and adhesive strengths [21]. But existing commercially bioadhesives, such as fibrin glue, show weak adhesiveness and lack of bioactivity [49]. In this study, a family of PPU-glues was developed and validated aiming to fulfill the requirements for post discectomy therapy.

Most importantly, adhesive strengths of PPU-glues were characterized *in vitro*, so as to explore the feasibility of AF seal before experiments *in vivo*. In view of the loading directions, both lap shear strength and burst pressure tests were conducted, the results of which reflected strong adhesive and cohesive strength of PPU-glue, suggesting that it could serve as a tissue adhesive

and a sealant simultaneously. In other words, the strong lap shear strength demonstrated the remote possibility of implant shedding, and the strong burst pressure indicated the high practicability of leak prevention. Compared with other reported adhesives for IVD therapy, PPU-glue showed stronger lap shear strength against porcine skin [50]. The adhesion strengths of bioadhesives were slightly lower after introducing polyphonels. The particle packing density is deemed to play a greater role in enhancing adhesive and cohesive strengths, but the mixing of TA diminished the particle packing density. Also, the chemical introduction of Cur also decreased the negative charge density of Cur-WPU$^-$ comparing with WPU$^-$ (Fig. 1C), thus decreased the electrostatic interaction between Cur-WPU$^-$ and WPU$^+$ nanoparticles. The results of radiological, histological and biomechanical experiments confirmed that PPU-glue could seal the AF defect and retain the NP tissue, which essentially benefited from strong tissue adhesiveness. Furthermore, the *in vitro* ramp-to-failure testing results on the bovine tail discs show that PPU-glue could resist the physiological upper bound of human intradiscal pressure (2.3 MPa). Thus, it is reasonable to believe that PPU-glues could provide sufficient sealing strength to prevent IVD re-herniation after discectomy on human beings.

Recently, it is reported that the combination of a glue and a patch was optimal for IVD repair [26]. However, starting from reality, patch is better suited as an AF mimetic in tissue engineered composites for total disc replacement to treat late-stage IVD degeneration [21], and many electrospun polymeric scaffolds have been developed to mimic the native AF lamellar structure [17,51,52]. By comparison, PPU-glue is more easily translatable to treat focal AF defects following discectomy and to treat early-stage or middle-stage IVD degeneration [21].

Notably, the adhesion strategy that combined a particle packing theory and an English ivy mechanism brings plentiful advantages besides strong adhesive strength. PPU-glue is injectable thanks to the form of aqueous dispersion before mixture, rendering it as a minimally invasive method. After mixing, it could gel rapidly without using any toxic chemical crosslinker, thereby reducing the time of surgery operation and the likelihood of cell disruption [53]. Additionally, the *in vitro* and the *in vivo* experiments results suggested that PPU-glue possessed good biocompatibility at both cellular and tissue levels. As known, excessive swelling will induce compression on adjacent tissues resulting in re-herniation [54], for instance, DuraSeal have the risks of tissue oppression and delocalization [55,56]. The results show minimal swelling behavior of PPU-glue, which is derived from inherent hydrophobicity and high crosslinking density. Considering the poor self-healing property of the IVDs, the ideal bioadhesives should avoid adhesion failure caused by fast degradation [57]. The results indicate slow degradation of PPU-glue *in vitro*, and it could maintain mechanical integrity long enough to allow tissue repair *in vivo*, despite there is no consensus on the optimal degradation property for IVD therapy. Moreover, pioneering study has reported it is biodegradable [28], and it can be tuned by various raw materials and processing conditions [58]. In addition, the results of swelling ratios, degradation rates and polyphenols release profiles collectively suggest that physical mixture of TA was looser than chemical bonding of Cur. TA mixing might diminish the packing density and the chemical introduction of Cur in the polymer backbone also weaken the electrostatic interaction as stated above. In a word, PPU-glue exhibited many intrinsic physicochemical properties brought by the adhesion strategy, which facilitated post discectomy therapy.

Superior bioactivity is another favorable feature of PPU-glue. As mentioned, ROS has been identified as a necessary mediator in the signaling network of disc cells, and excessive ROS can disturb the matrix metabolism and impair the mechanical function [44]. Therefore, we introduced polyphenols to endow the bioadhesives with ROS-scavenging capacity. Incidentally, TA is soluble in water and Cur has poor aqueous solubility [59,60] . Furthermore, the hydroxyl group of Cur can react with the isocyanate of waterborne polyurethane prepolymer, so we selected physical mixture and chemical bonding separately to introduce TA and Cur. After modification, there was no significant effect on the adhesive strength as mentioned above, because the adhesion strategy was not changed. As reported, TA and Cur have been commonly used as bioactive components in IVD biomaterials [37–41]. They can scavenge ROS in DPPH and ABTS solution [45,61], and attenuate oxidative stress in the TBHP-stimulated NPCs [39,48]. The results verify PPU-glue possessed sufficient ROS-scavenging capacity, which mainly derived from TA and further enhanced by Cur, similar to prior research [39]. Considering the slow degradation of PPU-glue, the ROS-scavenging capacity may last for some time when translated into the human clinical scenario, but the actual time needs further reasearch. The *in vitro* experiments confirmed the protective effects of PPU-glue on the degenerated NPCs, which could promote ECM anabolism and suppress ECM catabolism. The *in vivo* experiments further confirmed the therapeutic effects of PPU-glue on degenerated rat caudal discs; besides ECM metabolic balance, PPU-glue could maintain the disc height, morphology and structure, thereby promoting therapy biologically and biomechanically. In short, PPU-glue achieved considerable therapeutic effects for IVD degeneration.

Recent advances in therapeutic approaches highlight the significance of a combined strategy for AF repair and NP augmentation [22]. There is no doubt that the two-part biomaterial can meet the heterogeneity of the IVD hopefully, such as the combination of an AF sealant and a NP glue [26]. However, a multi-step process will enhance the operation difficulty. Our study decoupled the needs for AF seal and NP augmentation, and satisfied the needs correspondingly by adopting the adhesion strategy and the polyphenol-modified method, and finally attained the synergy effect only utilizing PPU-glue. As a result, PPU-glue possessed great application potential as an ideal candidate for post discectomy therapy.

Nonetheless, there are still several limitations in this study. Firstly, due to the granule structure of PPU-glue, it could only seal the AF defect instantly, but not form the lamellar structure like the native AF tissue directly. With the treatment prolonged, new AF tissue may gradually grow and eventually replace the bioadhesives *in situ*, but the actual effects need further verification. Secondly, the therapeutic mechanisms of PPU-glue worth in-depth study, given the prominent biological effects of TA and Cur, such as anti-inflammatory property [46,62–64]. Cur even could alleviate radiculopathy following IVD herniation [65,66]. Moreover, the modified method can be further optimized and extended, including drug selection, preparation and delivery [67,68]. Also, the cellular impacts of PPU-glue on AF cells should be investigated to better evaluate the cytotoxicity of PPU-glue in the repair of AF defect. Thirdly, there is no universally acknowledged animal model to evaluate therapeutic effects for discectomy. The reason why we selected the puncture-induced rat disc model is primarily considered the similar anatomical structures, namely AF defect and NP absence. Certainly, investigations of larger animals are necessary for the next study, and pain assessment should be incorporated into animal experiments as well. Hence, more rigorous and more comprehensive evaluations should be performed in the future work.

## 5. Conclusion

In this study, we successfully designed and synthesized a family of polyphenol-modified biomimetic bioadhesives for post discectomy therapy. PPU-glue offered the advantages as described below: fast gelation that reduced the operation time, minimal swelling behavior that avoided the overexpansion problem, tunable degradation rates that matched the poor self-healing prop-

erty, strong adhesive strength that benefited AF seal, superior antioxidant and anti-inflammatory properties that suppressed NP degeneration. PPU-glue also possessed good biocompatibility, prominent biological and biomechanical therapeutic effects.

In summary, the adhesion strategy that combined a particle packing theory and an English ivy mechanism was firstly applied to the IVD therapy field. The modified method of incorporating polyphenols was utilized to optimize the bioadhesives. The therapeutic approach was validated and the results show that PPU-glue could seal the AF defect and promote the NP augmentation effectively. Together, PPU-glue provided certain reference significance for post discectomy therapy, and its design principle could be universally expanded to the bioadhesives for other surgical uses.

## Declaration of competing interest

The authors declare that they have no known competing financial interests or personal relationships that could have appeared to influence the work reported in this paper.

## CRediT authorship contribution statement

**Yan Ju:** Writing – review & editing, Writing – original draft, Visualization, Validation, Software, Project administration, Methodology, Investigation, Formal analysis, Data curation. **Shiyuan Ma:** Validation, Software, Methodology, Investigation. **Meimei Fu:** Visualization, Validation, Methodology, Investigation. **Min Wu:** Validation, Methodology, Investigation. **Yue Li:** Visualization, Methodology, Investigation. **Yue Wang:** Visualization, Methodology, Investigation. **Meihan Tao:** Validation, Supervision, Project administration, Methodology. **Zhihui Lu:** Resources, Funding acquisition, Conceptualization. **Jinshan Guo:** Writing – review & editing, Supervision, Resources, Project administration, Funding acquisition, Conceptualization.

## Acknowledgements

This work was supported by the Natural Science Foundation of China (Grant Nos. 82272453, U21A2099, and 82102545), the Youth Talent of Guangdong Special Support Program (0620220207), the Guangdong Basic and Applied Basic Research Foundation (Grant No. 2024A1515012664) and the Open Program from Guangdong Provincial Key Laboratory of Bone and Joint Degeneration Disease.

## Supplementary materials

Supplementary material associated with this article can be found, in the online version, at doi:10.1016/j.actbio.2024.09.038.

## References

[1] J. Hartvigsen, M.J. Hancock, A. Kongsted, Q. Louw, M.L. Ferreira, S. Genevay, D. Hoy, J. Karppinen, G. Pransky, J. Sieper, R.J. Smeets, M. Underwood, Lancet Low Back Pain Series Working Group, What low back pain is and why we need to pay attention, Lancet 391 (10137) (2018) 2356–2367.
[2] Y. Takeoka, T. Yurube, K. Morimoto, S. Kunii, Y. Kanda, R. Tsujimoto, Y. Kawakami, N. Fukase, T. Takemori, K. Omae, Y. Kakiuchi, S. Miyazaki, K. Kakutani, T. Takada, K. Nishida, M. Fukushima, R. Kuroda, Reduced nucleotomy-induced intervertebral disc disruption through spontaneous spheroid formation by the low adhesive scaffold collagen (LASCol), Biomaterials 235 (2020) 119781.
[3] A. Zhang, Z. Cheng, Y. Chen, P. Shi, W. Gan, Y. Zhang, Emerging tissue engineering strategies for annulus fibrosus therapy, Acta Biomater. 167 (2023) 1–15.
[4] F. Ye, F.J. Lyu, H. Wang, Z. Zheng, The involvement of immune system in intervertebral disc herniation and degeneration, JOR Spine 5 (1) (2022) e1196.
[5] I.L.M. Isa, S.L. Teoh, N.H.M. Nor, S.A. Mokhtar, Discogenic low back pain: anatomy, pathophysiology and treatments of intervertebral disc degeneration, Int. J. Mol. Sci. 24 (1) (2023) 208.
[6] T. Benzakour, V. Igoumenou, A.F. Mavrogenis, A. Benzakour, Current concepts for lumbar disc herniation, Int. Orthop. 43 (4) (2019) 841–851.
[7] D. Zhou, H. Liu, Z. Zheng, D. Wu, Design principles in mechanically adaptable biomaterials for repairing annulus fibrosus rupture: a review, Bioact. Mater. 31 (2024) 422–439.
[8] H. Kanno, T. Aizawa, K. Hahimoto, E. Itoi, Minimally invasive discectomy for lumbar disc herniation: current concepts, surgical techniques, and outcomes, Int. Orthop. 43 (4) (2019) 917–922.
[9] F. Han, Q. Yu, G. Chu, J. Li, Z. Zhu, Z. Tu, C. Liu, W. Zhang, R. Zhao, H. Mao, F. Han, B. Li, Multifunctional nanofibrous scaffolds with angle-ply microstructure and co-delivery capacity promote partial repair and total replacement of intervertebral disc, Adv. Healthc. Mater. 11 (19) (2022) 2200895.
[10] Y. Moriguchi, B. Borde, C. Berlin, C. Wipplinger, S.R. Sloan, S. Kirnaz, B. Pennicooke, R. Navarro-Ramirez, T. Khair, P. Grunert, E. Kim, L. Bonassar, R. Hartl, *In vivo* annular repair using high-density collagen gel seeded with annulus fibrosus cells, Acta Biomater. 79 (2018) 230–238.
[11] G.T. Desmoulin, V. Pradhan, T.E. Milner, Mechanical aspects of intervertebral disc injury and implications on biomechanics, Spine 45 (8) (2020) E457–E464.
[12] Q. Meng, E. Xie, H. Sun, H. Wang, J. Li, Z. Liu, K. Li, J. Hu, Q. Chen, C. Liu, B. Li, F. Han, High-strength smart microneedles with "offensive and defensive" effects for intervertebral disc repair, Adv. Mater. 36 (2) (2023) 2305468.
[13] N. Shepard, W. Cho, Recurrent lumbar disc herniation: a review, Glob. Spine J. 9 (2) (2019) 202–209.
[14] K. Ono, K. Ohmori, R. Yoneyama, O. Matsushige, T. Majima, Risk factors and surgical management of recurrent herniation after full-endoscopic lumbar discectomy using interlaminar approach, J. Clin. Med. 11 (3) (2022) 748.
[15] C. Tanavalee, W. Limthongkul, W. Yingsakmongkol, P. Luksanapruksa, W. Singhatanadgige, A comparison between repeat discectomy versus fusion for the treatment of recurrent lumbar disc herniation: systematic review and meta–analysis, J. Clin. Neurosci. 66 (2019) 202–208.
[16] Q. Wei, D. Liu, G. Chu, Q. Yu, Z. Liu, J. Li, Q. Meng, W. Wang, F. Han, B. Li, TGF–beta1-supplemented decellularized annulus fibrosus matrix hydrogels promote annulus fibrosus repair, Bioact. Mater. 19 (2023) 581–593.
[17] Q. Yu, F. Han, Z. Yuan, Z. Zhu, C. Liu, Z. Tu, Q. Guo, R. Zhao, W. Zhang, H. Wang, H. Mao, B. Li, C. Zhu, Fucoidan-loaded nanofibrous scaffolds promote annulus fibrosus repair by ameliorating the inflammatory and oxidative microenvironments in degenerative intervertebral discs, Acta Biomater. 148 (2022) 73–89.
[18] J. Bian, F. Cai, H. Chen, Z. Tang, K. Xi, J. Tang, L. Wu, Y. Xu, L. Deng, Y. Gu, W. Cui, L. Chen, Modulation of local overactive inflammation via injectable hydrogel microspheres, Nano Lett. 21 (6) (2021) 2690–2698.
[19] Y. Xu, Y. Gu, F. Cai, K. Xi, T. Xin, J. Tang, L. Wu, Z. Wang, F. Wang, L. Deng, C.L. Pereira, B. Sarmento, W. Cui, L. Chen, Metabolism balance regulation via antagonist-functionalized injectable microsphere for nucleus pulposus regeneration, Adv. Funct. Mater. 30 (52) (2020) 2006333.
[20] G. Song, Z. Qian, X. Liu, B. Chen, G. Li, Z. Wang, K. Wang, Z. Zou, F. Galbusera, M. Domingos, L. Ren, H.J. Wilke, L. Ren, Bioinspired intervertebral disc with multidirectional stiffness prepared via multimaterial additive manufacturing, Adv. Funct. Mater. 33 (44) (2023) 2300298.
[21] T.J. DiStefano, J.O. Shmukler, G. Danias, J.C. Iatridis, The functional role of interface tissue engineering in annulus fibrosus repair: bridging mechanisms of hydrogel integration with regenerative outcomes, ACS Biomater. Sci. Eng. 6 (12) (2020) 6556–6586.
[22] S.R. Sloan, C. Wipplinger, S. Kirnaz, R. Navarro-Ramirez, F. Schmidt, D. McCloskey, T. Pannellini, A. Schiavinato, R. Härtl, L.J. Bonassar, Combined nucleus pulposus augmentation and annulus fibrosus repair prevents acute intervertebral disc degeneration after discectomy, Sci. Transl. Med. 12 (534) (2020) eaay2380.
[23] S. Tarafder, G.Y. Park, J. Felix, C.H. Lee, Bioadhesives for musculoskeletal tissue regeneration, Acta Biomater. 117 (2020) 77–92.
[24] W. Zhu, Y.J. Chuah, D.A. Wang, Bioadhesives for internal medical applications: a review, Acta Biomater. 74 (2018) 1–16.
[25] M. Zhang, J. Liu, T. Zhu, H. Le, X. Wang, J. Guo, G. Liu, J. Ding, Functional macromolecular adhesives for bone fracture healing, ACS Appl. Mater. Interfaces 14 (1) (2022) 1–19.
[26] X. Li, Y. Liu, L. Li, R. Huo, F. Ghezelbash, Z. Ma, G. Bao, S. Liu, Z. Yang, M.H. Weber, N.Y.K. Li-Jessen, L. Haglund, J. Li, Tissue-mimetic hybrid bioadhesives for intervertebral disc repair, Mater. Horiz. 10 (5) (2023) 1705–1718.
[27] T.J. DiStefano, J.O. Shmukler, G. Danias, T. Di Pauli von Treuheim, W.W. Hom, D.A. Goldberg, D.M. Laudier, P.R. Nasser, A.C. Hecht, S.B. Nicoll, J.C. Iatridis, Development of a two-part biomaterial adhesive strategy for annulus fibrosus repair and *ex vivo* evaluation of implant herniation risk, Biomaterials 258 (2020) 120309.
[28] Q. Li, W. Song, J. Li, C. Ma, X. Zhao, J. Jiao, O. Mrowczynski, B.S. Webb, E.B. Rizk, D. Lu, C. Liu, Bioinspired super-strong aqueous synthetic tissue adhesives, Matter 5 (3) (2022) 933–956.
[29] K. Wu, Y. Zhao, M. Wu, Y. Li, Z. Hu, Z. Lu, J. Guo, Development and applications of polymeric biomimetic tissue adhesives, J. Funct. Polym. 34 (2) (2021) 93–113.
[30] Y. Huang, Y. Wang, L. Tan, L. Sun, J. Petrosino, M. Cui, F. Hao, M. Zhang, Nanospherical arabinogalactan proteins are a key component of the high-strength adhesive secreted by English ivy, Proc. Natl. Acad. Sci. USA 113 (23) (2016) E3193–E3202.
[31] D. Wu, G. Li, X. Zhou, W. Zhang, H. Liang, R. Luo, K. Wang, X. Feng, Y. Song, C. Yang, Repair strategies and bioactive functional materials for intervertebral disc, Adv. Funct. Mater 32 (52) (2022) 2209471.
[32] J. Shen, A. Chen, Z. Cai, Z. Chen, R. Cao, Z. Liu, Y. Li, J. Hao, Exhausted local lactate accumulation via injectable nanozyme-functionalized hydrogel micro-

sphere for inflammation relief and tissue regeneration, Bioact. Mater. 12 (2022) 153–168.
[33] C. Liu, L. Fan, M. Guan, Q. Zheng, J. Jin, X. Kang, Z. Gao, X. Deng, Y. Shen, G. Chu, J. Chen, Z. Yu, L. Zhou, Y. Wang, A redox homeostasis modulatory hydrogel with GLRX3(+) extracellular vesicles attenuates disc degeneration by suppressing nucleus pulposus cell senescence, ACS Nano 17 (14) (2023) 13441–13460.
[34] S. Wu, Y. Shi, L. Jiang, W. Bu, K. Zhang, W. Lin, C. Pan, Z. Xu, J. Du, H. Chen, H. Wang, N-acetylcysteine-derived carbon dots for free radical scavenging in intervertebral disc degeneration, Adv. Healthc. Mater. 12 (24) (2023) 2300533.
[35] Y. Li, Y. Miao, L. Yang, Y. Zhao, K. Wu, Z. Lu, Z. Hu, J. Guo, Recent advances in the development and antimicrobial applications of metal-phenolic networks, Adv. Sci. 9 (27) (2022) 2202684.
[36] X. Gao, Z. Xu, G. Liu, J. Wu, Polyphenols as a versatile component in tissue engineering, Acta Biomater. 119 (2021) 57–74.
[37] K. Wu, M. Fu, Y. Zhao, E. Gerhard, Y. Li, J. Yang, J. Guo, Anti-oxidant anti-inflammatory and antibacterial tannin-crosslinked citrate-based mussel-inspired bioadhesives facilitate scarless wound healing, Bioact. Mater. 20 (2023) 93–110.
[38] Y. Wang, M. Deng, Y. Wu, C. Hu, B. Zhang, C. Guo, H. Song, Q. Kong, Y. Wang, Sustained gene delivery from inflammation-responsive anti-inflammatory hydrogels promotes extracellular matrix metabolism balance in degenerative nucleus pulposus, Compos. B Eng. 236 (2022) 109806.
[39] Y. Wang, Y. Wu, B. Zhang, C. Zheng, C. Hu, C. Guo, Q. Kong, Y. Wang, Repair of degenerative nucleus pulposus by polyphenol nanosphere-encapsulated hydrogel gene delivery system, Biomaterials 298 (2023) 122132.
[40] A. Larrañaga, I.L.M. Isa, V. Patil, S. Thamboo, M. Lomora, M.A. Fernández-Yague, J.R. Sarasua, C.G. Palivan, A. Pandit, Antioxidant functionalized polymer capsules to prevent oxidative stress, Acta Biomater. 67 (2018) 21–31.
[41] F. Zamboni, G. Ren, M. Culebras, J. O'Driscoll, J. O'Dwyer, E.J. Ryan, M.N. Collins, Curcumin encapsulated polylactic acid nanoparticles embedded in alginate/gelatin bioinks for *in situ* immunoregulation: characterization and biological assessment, Int. J. Biol. Macromol. 221 (2022) 1218–1227.
[42] A. Lai, J. Gansau, S.E. Gullbrand, J. Crowley, C. Cunha, S. Dudli, J.B. Engiles, M. Fusellier, R.M. Goncalves, D. Nakashima, J. Okewunmi, M. Pelletier, S.M. Presciutti, J. Schol, Y. Takeoka, S. Yang, T. Yurube, Y. Zhang, J.C. Iatridis, Development of a standardized histopathology scoring system for intervertebral disc degeneration in rat models: an initiative of the ORS spine section, JOR Spine 4 (2) (2021) e1150.
[43] Y. Li, L. Chen, Y. Gao, X. Zou, F. Wei, Oxidative stress and intervertebral disc degeneration: pathophysiology, signaling pathway, and therapy, Oxid. Med. Cell. Longev. 2022 (2022) 1984742.
[44] C. Feng, M. Yang, M. Lan, C. Liu, Y. Zhang, B. Huang, H. Liu, Y. Zhou, ROS: crucial intermediators in the pathogenesis of intervertebral disc degeneration, Oxid. Med. Cell. Longev. (2017) (2017) 5601593.
[45] Y. Li, Y. Miao, L. Yang, G. Wang, M. Fu, Y. Wang, D. Fu, J. Huang, J. Wang, Z. Fan, Z. Lu, J. Guo, Z. Hu, Malate-based polyester chemically shielded metal-phenolic networks coated artificial hair fibers with long-lasting antimicrobial and anti-inflammatory performance, Chem. Eng. J. 455 (2023) 140572.
[46] M. Fu, Y. Zhao, Y. Wang, Y. Li, M. Wu, Q. Liu, Z. Hou, Z. Lu, K. Wu, J. Guo, On-demand removable self-healing and pH-responsive europium-releasing adhesive dressing enables inflammatory microenvironment modulation and angiogenesis for diabetic wound healing, Small 19 (3) (2023) 2205489.
[47] L. Kang, Q. Xiang, S. Zhan, Y. Song, K. Wang, K. Zhao, S. Li, Z. Shao, C. Yang, Y. Zhang, Restoration of autophagic flux rescues oxidative damage and mitochondrial dysfunction to protect against intervertebral disc degeneration, Oxid. Med. Cell. Longev. (2019) (2019) 7810320.
[48] G. Zheng, Z. Pan, Y. Zhan, Q. Tang, F. Zheng, Y. Zhou, Y. Wu, Y. Zhou, D. Chen, J. Chen, X. Wang, W. Gao, H. Xu, N. Tian, X. Zhang, TFEB protects nucleus pulposus cells against apoptosis and senescence via restoring autophagic flux, Osteoarthr. Cartil. 27 (2) (2019) 347–357.
[49] H. Zhu, J. Tian, H. Mao, Z. Gu, Bioadhesives: current hotspots and emerging challenges, Curr. Opin. Biomed. Eng. 18 (2021) 100271.
[50] R. Yang, B. Wang, X. Zhang, Y. Sun, Y. Zhang, Z. Xu, Q. Yang, W. Liu, A nucleobase-driven self-gelled hyaluronic acid-based injectable adhesive hydrogel enhances intervertebral disc repair, Adv. Funct. Mater. 34 (36) (2024) 2401232, doi:10.1002/adfm.202401232.
[51] J. Yang, L. Wang, W. Zhang, Z. Sun, Y. Li, M. Yang, D. Zeng, B. Peng, W. Zheng, X. Jiang, G. Yang, Reverse reconstruction and bioprinting of bacterial cellulose-based functional total intervertebral disc for therapeutic implantation, Small 14 (7) (2018) 1702582.
[52] C. Zhu, J. Li, C. Liu, P. Zhou, H. Yang, B. Li, Modulation of the gene expression of annulus fibrosus-derived stem cells using poly(ether carbonate urethane)urea scaffolds of tunable elasticity, Acta Biomater. 29 (2016) 228–238.
[53] C.J. Panebianco, T.J. DiStefano, B. Mui, W.W. Hom, J.C. Iatridis, Crosslinker concentration controls TGF$\beta$-3 release and annulus fibrosus cell apoptosis in genipin-crosslinked fibrin hydrogels, Eur. Cell Mater. 39 (2020) 211–226.
[54] W. Feng, Z. Wang, Tailoring the swelling-shrinkable behavior of hydrogels for biomedical applications, Adv. Sci. 41 (2023) 2303326.
[55] H. Zhu, X. Mei, Y. He, H. Mao, W. Tang, R. Liu, J. Yang, K. Luo, Z. Gu, L. Zhou, Fast and high strength soft tissue bioadhesives based on a peptide dendrimer with antimicrobial properties and hemostatic ability, ACS Appl. Mater. Interfaces 12 (4) (2020) 4241–4253.
[56] Y. Mizuno, T. Taguchi, Fish gelatin-based absorbable dural sealant with anti-inflammatory properties, ACS Biomater. Sci. Eng. 7 (10) (2021) 4991–4998.
[57] J. Guo, G. Kim, D. Shan, J.P. Kim, J. Hu, W. Wang, F.G. Hamad, G. Qian, E.B. Rizk, J. Yang, Click chemistry improved wet adhesion strength of mussel-inspired citrate-based antimicrobial bioadhesives, Biomaterials 112 (2017) 275–286.
[58] A. Magnin, E. Pollet, V. Phalip, L. Avérous, Evaluation of biological degradation of polyurethanes, Biotechnol. Adv. 39 (2020) 107457.
[59] O. Naksuriya, S. Okonogi, R.M. Schiffelers, W.E. Hennink, Curcumin nanoformulations: a review of pharmaceutical properties and preclinical studies and clinical data related to cancer treatment, Biomaterials 35 (10) (2014) 3365–3383.
[60] R. Chen, J.L. Funnell, G.B. Quinones, M. Bentley, J.R. Capadona, R.J. Gilbert, E.F. Palermo, Poly(pro-curcumin) materials exhibit dual release rates and prolonged antioxidant activity as thin films and self-assembled particles, Biomacromolecules 24 (1) (2023) 294–307.
[61] J. Qu, X. Zhao, Y. Liang, T. Zhang, P.X. Ma, B. Guo, Antibacterial adhesive injectable hydrogels with rapid self-healing, extensibility and compressibility as wound dressing for joints wound healing, Biomaterials 183 (2018) 185–199.
[62] Y. Zhao, J. Li, L. Liu, Y. Wang, Y. Ju, C. Zeng, Z. Lu, D. Xie, J. Guo, Zinc-based tannin-modified composite microparticulate scaffolds with balanced antimicrobial activity and osteogenesis for infected bone defect repair, Adv. Healthc. Mater. 12 (20) (2023) 2300303.
[63] N. Ninan, A. Forget, V.P. Shastri, N.H. Voelcker, A. Blencowe, Antibacterial and anti-inflammatory pH-responsive tannic acid-carboxylated agarose composite hydrogels for wound healing, ACS Appl. Mater. Interfaces 8 (42) (2016) 28511–28521.
[64] D. Zheng, C. Huang, H. Huang, Y. Zhao, M.R.U. Khan, H. Zhao, L. Huang, Antibacterial mechanism of curcumin: a review, Chem. Biodivers. 17 (8) (2020) 2000171.
[65] T. Ma, C.J. Guo, X. Zhao, L. Wu, S.X. Sun, Q.H. Jin, The effect of curcumin on NF-$\kappa$B expression in rat with lumbar intervertebral disc degeneration, Eur. Rev. Med. Pharmacol. Sci. 19 (7) (2015) 1305–1314.
[66] L. Xiao, M. Ding, A. Fernandez, P. Zhao, L. Jin, X. Li, Curcumin alleviates lumbar radiculopathy by reducing neuroinflammation, oxidative stress and nociceptive factors, Eur. Cell Mater. 33 (2017) 279–293.
[67] Y. Guo, Q. Sun, F. Wu, Y. Dai, X. Chen, Polyphenol-containing nanoparticles: synthesis, properties, and therapeutic delivery, Adv. Mater. 33 (22) (2021) 2007356.
[68] Z. Chen, M.A. Farag, Z. Zhong, C. Zhang, Y. Yang, S. Wang, Y. Wang, Multifaceted role of phyto-derived polyphenols in nanodrug delivery systems, Adv. Drug Deliv. Rev. 176 (2021) 113870.